Spectroscopic study of Y b^{3+} centres in the Y $Al_3(BO_3)_4$ nonlinear laser crystal

2003 J. Phys.: Condens. Matter 15 7789

(http://iopscience.iop.org/0953-8984/15/45/017)

INSTITUTE OF PHYSICS PUBLISHING JOURNAL OF PHYSICS: CONDENSED MATTER

J. Phys.: Condens. Matter **15** (2003) 7789–7801 PII: S0953-8984(03)64009-9

Spectroscopic study of Yb^{3+} centres in the $YAl_3(BO_3)_4$ nonlinear laser crystal

M O Ramírez[1,4], L E Bausá[1], D Jaque[1], E Cavalli[2], A Speghini[3] and M Bettinelli[3]

[1] Departamento Física de Materiales, Universidad Autónoma de Madrid, 28049 Madrid, Spain
[2] INFM and Dipartimento di Chimica Generale ed Inorganica, Chimica Analitica e Chimica Fisica, Università di Parma, Parco Area delle Scienze 17/a, 43100 Parma, Italy
[3] Dipartimento Scientifico e Tecnologico, University of Verona and INSTM, UdR Verona, Ca' Vignal, Strada Le Grazie 15, 37134 Verona, Italy

E-mail: mariola.ramirez@uam.es

Received 26 May 2003
Published 31 October 2003
Online at stacks.iop.org/JPhysCM/15/7789

Abstract

A spectroscopic study of Yb^{3+} ions in $YAl_3(BO_3)_4$ laser crystals is presented. Polarized absorption and site selective spectroscopy experiments at low temperature have been used to determine the presence of two different Yb^{3+} centres in this host crystal in the concentration range 0.2–9 at.%. The contribution of these centres to the absorption spectra has been found to be dependent on the total Yb^{3+} concentration, and the Stark energy level diagrams corresponding to the different Yb^{3+} centres have been determined. The importance of electron–phonon coupling in the optical transitions of Yb^{3+} ions has been also pointed out.

1. Introduction

Yb^{3+} ion is one of the most interesting optically active ions that can be used nowadays in a solid state laser material. It shows several advantages over other trivalent rare earth ions which make it especially attractive. Yb^{3+} ion has only two levels ($^2F_{7/2}$ ground and $^2F_{5/2}$ excited states) separated by an energy of around 10 000 cm^{-1}, allowing optical pumping with commercial diodes operating around 980 nm. Its small ionic radius (due to lanthanide contraction) is very similar to that of Y^{3+} and leads to the possibility of obtaining high Yb^{3+} doping levels. The electronic configuration of Yb^{3+} ion is $4f^{13}$, hence the 4f electrons are less shielded than in other ions of the series, leading to important electron–phonon coupling [1, 2]. As a result, Yb^{3+} ions show relatively broad absorption and emission bands, which offer the possibility of infrared tunability and the generation of ultrashort pulses [3–5]. On the other hand, the

[4] Author to whom any correspondence should be addressed.

Yb^{3+} ion presents a long radiative lifetime value and high quantum efficiency, so that the pump induced crystal heating during laser operation is efficiently reduced. These features make Yb^{3+} an excellent laser emitting centre, and consequently, the study of nonlinear crystals as host matrices for this ion is receiving considerable attention in order to develop small and compact diode pumped solid state lasers emitting simultaneously in the near infrared and in the visible spectral domain.

In this sense, yttrium aluminium borate $YAl_3(BO_3)_4$ (YAB), has been demonstrated to be a very good laser host crystal because of its good mechanical strength and thermal conductivity among other factors [6–8]. Due to its excellent nonlinear coefficients, simultaneous laser action in the red, green and blue regions have been previously reported in Nd:YAB under near infrared pumping [9, 10]. In the case of Yb:YAB, efficient and tunable cw laser operation at around 1040 nm has been demonstrated under diode pumping [11, 12] and additionally, cw coherent green radiation inside the tunable range 513–546 nm has been obtained with a high quality beam and high output power, 1.1 W. To the best of our knowledge, this value corresponds to the highest green power achieved by a self-frequency doubling crystal [13]. More recently, laser light generation in the 560–570 nm yellow spectral region has also been obtained in a coupled cavity Yb:YAB microchip laser [14, 15].

The spectroscopic studies on Yb:YAB have been mainly carried out at room temperature in order to determine the main parameters involved in laser action [16]. However, in spite of the great potential of this system, the information reported up to now on the low temperature (LT) spectroscopy can be considered as preliminary. Several aspects concerning the LT absorption spectra, such as their polarization character, the concentration effects, or a possible multisite distribution, have not yet been, to the best of our knowledge, the subject of attention. Since a deeper knowledge of the optical spectroscopy of this system is a fundamental key in the understanding and future optimization of the infrared and visible laser gains, the purpose of this paper is to obtain a deep insight into the optical spectroscopy of Yb^{3+} in YAB. LT polarized absorption spectra have been studied for different Yb^{3+} concentrations, and by comparing the LT σ and π absorption spectra, the character of the Stark sublevels corresponding to the $^2F_{5/2}$ excited state has been determined. From the analysis of the LT absorption spectra, two different Yb^{3+} centres have been detected, and their relative distribution has been determined in a wide range of Yb^{3+} concentration (0.2–9 at.%). Site selective spectroscopy experiments have confirmed the presence of these two centres and allowed the determination of the Stark sublevels of the $^2F_{7/2}$ and $^2F_{5/2}$ states.

2. Experimental details

Different Yb^{3+}:YAB single crystals were grown by spontaneous nucleation from $K_2Mo_3O_{10}$ and B_2O_3 flux [17]. Yb_2O_3 was added to obtain different Yb^{3+} doping levels (see table 1). The 1% and 5% doped crystals (Yb/Y%), were slightly co-doped with Nd^{3+} (0.2 and 0.1% respectively) in order to analyse the effect of co-doping on the Yb^{3+} spectra. The actual Yb^{3+} concentrations in the crystals were determined by total x-ray fluorescence.

The LT absorption spectra were measured at 10 K with a spectroscopic system equipped with a 300 W halogen lamp fitted with a 0.25 m Spex monochromator as the source, and a 1.26 m Spex monochromator with a EMI TE9684QB NIR extended photomultiplier to analyse and detect the output radiation.

The luminescence spectra have been obtained by using an argon pumped Ti:sapphire laser (Spectra Physics, model 3900) as the excitation source. The luminescence was detected using a calibrated germanium detector or a cooled photomultiplier. The emitted light was focused on the entrance slit of a monochromator (SPEX 500M) and recorded with an EG&G lock-in

Table 1. Different samples used in this work indicating the nominal ytterbium to yttrium concentration in the crystal.

Sample	$[Yb^{3+}]/[Y^{3+}]$ (%)
1	0.265
2	1 (0.2 Nd^{3+})
3	2.65
4	5 (0.1 Nd^{3+})
5	7
6	8.9

Table 2. Decomposition of the $^2F_{7/2}$ and $^2F_{5/2}$ states of Yb^{3+} free ion into D_3 symmetry and the electric dipole selection rules (double group notation).

Spherical symmetry	D_3 symmetry
$^2F_{5/2}$	$2E_{1/2} + E_{3/2}$
$^2F_{7/2}$	$3E_{1/2} + E_{3/2}$
Selection rules	Polarization
$E_{1/2} \rightarrow E_{1/2}$	σ, π
$E_{1/2} \rightarrow E_{3/2}$	σ
$E_{3/2} \rightarrow E_{3/2}$	π

amplifier. The measurements at LT (10 K) were performed by using a Leybold–Heraeus closed cycle He cryostat.

The resolution for the absorption and luminescence measurements was around 0.2 nm.

3. Results and discussion

3.1. Absorption spectra

The study of the LT (10 K) absorption spectra allows us to identify the position and character of the crystal field transitions starting from the lowest energy Stark sublevel of the $^2F_{7/2}$ ground state up to the different Stark sublevels of the $^2F_{5/2}$ excited state of Yb^{3+} ions in YAB.

YAB crystals belong to the trigonal system with space group $R32$ (huntite structure) and cell parameters $a = b = 9.295$ Å and $c = 7.243$ Å [18]. In this host RE^{3+} ions usually enter at Y^{3+} lattice sites with six-fold oxygen coordination and trigonal prismatic geometry with D_3 point symmetry [19]. Within this consideration, it is expected that this D_3 symmetry splits the two free ion energy states, $^2F_{7/2}$ and $^2F_{5/2}$, into four and three doubly degenerate crystal field levels (Kramer doublets), respectively, their character being $E_{1/2}$ or $E_{3/2}$, as follows from group theory [20]. In particular, the $^2F_{5/2}$ excited state splits into two $E_{1/2}$ and one $E_{3/2}$ doubly degenerate levels, whereas the $^2F_{7/2}$ fundamental state splits into three $E_{1/2}$ and one $E_{3/2}$ doubly degenerate levels, as is summarized in table 2. In our case, the LT absorption spectra can be well analysed on this basis.

Figure 1 shows the polarized absorption spectra of Yb^{3+}:YAB (sample 3) obtained at LT for two different configurations: σ configuration, with the electric field of the incoming beam perpendicular to the c crystal axis of the sample, ($E \perp c$), and π configuration with the electric field of the incident beam parallel to the c axis, ($E \parallel c$). The σ spectrum displayed in figure 1 is consistent with the LT α spectrum (light beam parallel to the c axis of the sample) reported by Földvári *et al* [21]. This fact confirms that the spectra are dominated by electric dipole induced

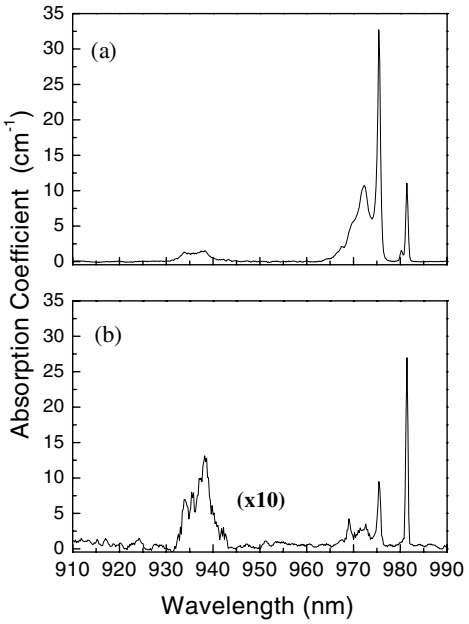

Figure 1. (a) σ and (b) π polarized absorption spectra of Yb:YAB (sample 3) at liquid helium temperature.

transitions, since the determinant feature to specify the selection rules is the orientation of the electric field of the light beam relative to the *c* axis of the crystal. Information on the particular character of the involved crystal field transitions can be obtained by comparing the LT σ and π polarized spectra and by taking into consideration the electric dipole selection rules reported in table 2.

The σ polarized spectrum in figure 1 shows three structured bands (absorption regions). These structured bands can be associated with transitions from the lowest Stark level (0) of the $^2F_{7/2}$ ground state to the three Stark components ($0'$, $1'$, $2'$, in increasing energy order) of the $^2F_{5/2}$ excited state. They appear centred at 935 nm ($0 \rightarrow 2'$), 975 nm ($0 \rightarrow 1'$), and 981 nm ($0 \rightarrow 0'$). By comparing the σ and π spectra a main feature is observed: the central absorption band at 975 nm in the σ spectrum is strongly reduced (by a factor of 50) in the π polarization, whereas the remaining bands are observed for both polarizations with comparable intensities. Group theory can be applied to obtain the electric dipole selection rules, assuming D_3 symmetry. See table 2.

Taking into account those selection rules, the character of the three Stark sublevels of the excited state, as well as that of the lowest Stark sublevel of the ground state, can be obtained. Since there is not any pure π polarized transition, it can be concluded that the character of the $^2F_{7/2}(0)$ Stark level of the ground state is $E_{1/2}$ and those corresponding to the three Stark sublevels of the $^2F_{5/2}$ excited state are $E_{1/2}$, $E_{3/2}$ and $E_{1/2}$, in order of increasing energy.

An inspection of the polarized absorption spectra reveals that the three transition regions from the lowest energy Stark level do not correspond, in any case, to single lines.

Firstly, a clear structure and an important broadening are present in the $^2F_{7/2}(0) \rightarrow {}^2F_{5/2}(1', 2')$ transitions (peaking at 935 and 975 nm, receptively). This structure can be related to vibronic transitions involving split components of the $^2F_{5/2}$ excited state. As pointed out in most of Yb^{3+} doped crystals, strong electron–phonon interaction takes place, and the electronic transitions are accompanied by vibronic sidebands which in some cases could

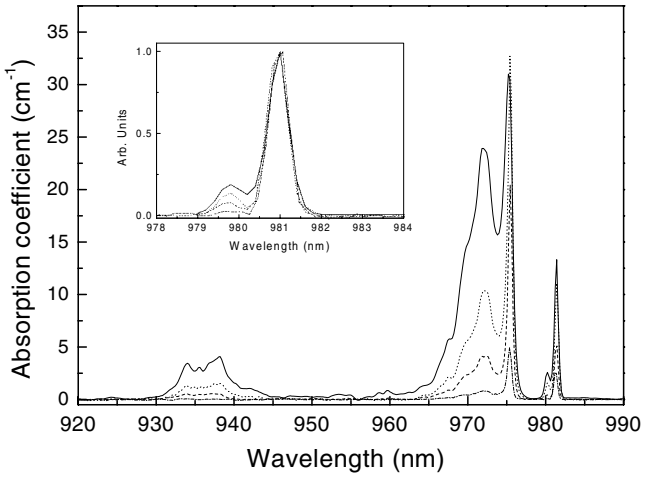

Figure 2. LT (10 K) σ-polarized absorption spectra of Yb:YAB for different Yb^{3+} concentrations. Solid curve: sample 6; dotted curve: sample 3; dashed curve: sample 2; dotted–dashed curve: sample 1. The inset shows a detail of the absorption spectra normalized at $\lambda = 981.4$ nm.

exceed and mask the zero-phonon transitions probabilities [22–24]. Secondly, a clear doublet structure around 980 nm is observed in the spectra for both polarizations. Two sharp peaks, located at 981.4 and 980.2 nm, appear in the region associated to the $^2F_{7/2}(0) \rightarrow {}^2F_{5/2}(0')$ transition. Some previous work [15, 21] have already evidenced this doublet structure, but up to now its origin has not been determined. As will be shown later, this structure can be related to the presence of different Yb^{3+} centres in the YAB crystal.

Finally, two very weak peaks at 975.2 and 969 nm (10 254 and 10 319 cm^{-1}) emerge in the π polarized spectrum (though they can be also masked in the σ spectrum). They could be, in principle, due to the first and second phonon replica of the $^2F_{7/2}(0) \rightarrow {}^2F_{5/2}(0')$ zero-phonon low energy peak (10 188 cm^{-1}), since the consecutive energy difference among them is the same (65 cm^{-1}) and selective excitation experiments have not shown different results. Unfortunately, the detection of such a low energy lattice phonon in the Raman spectra has not yet been reported due to the experimental limitations, and different techniques should be used to confirm this assignment.

3.1.1. Concentration effects. The LT polarized absorption spectra have been studied in a wide range of Yb^{3+} concentrations (see table 1). Figure 2 shows, for the sake of clarity, the σ polarized absorption spectra obtained at LT (10 K) for just four of the different nominal Yb^{3+} concentrations analysed in this work and corresponding to samples 1, 2, 3 and 6 listed in table 1.

Before going into the effect of Yb^{3+} concentration on the absorption spectra, it is important to determine the actual ytterbium concentration in the samples. Figure 3(a) shows the results obtained from the total x-ray fluorescence analysis. As observed, a linear dependence on the nominal ytterbium concentration is obtained in the whole range studied. The segregation coefficient can be determined from the linear regression to be 0.92, very close to one, which indicates the good incorporation of Yb^{3+} ions into the YAB host crystal.

On the other hand, figure 3(b) shows the total area under the LT σ absorption spectra as a function of ytterbium concentration in the crystals, for all the samples used in this work. Again, a linear dependence is obtained. This result can be a useful tool to determined Yb^{3+} concentration in the crystals from the absorption spectra.

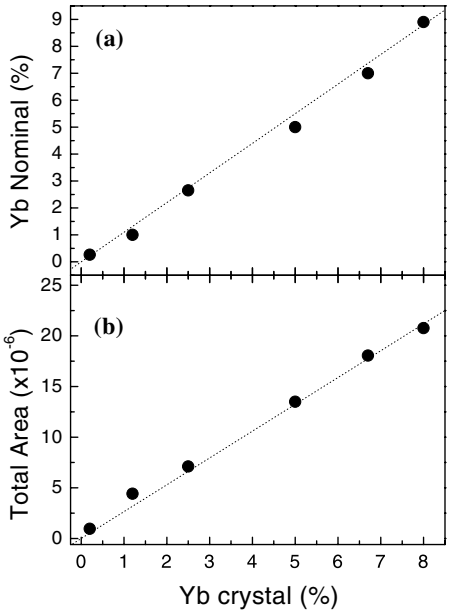

Figure 3. (a) Ytterbium concentration in melt versus ytterbium concentration in crystal; (b) LT absorption area as a function of ytterbium concentration in the crystal.

The analysis of the absorption spectra as a function of the Yb^{3+} concentration dependence reveals interesting information.

One of the most relevant results from figure 2 can be obtained from the behaviour of the doublet structure around 980 nm, the $^2F_{7/2}(0) \rightarrow {}^2F_{5/2}(0')$ transition. As a matter of fact, the relative intensities of the two narrow lines peaking at 981.4 and 980.2 nm change with ytterbium content in the samples. This can be clearly observed in the inset of figure 2 where a detail of the absorption spectra in the region associated with the $^2F_{5/2}(0) \rightarrow {}^2F_{7/2}(0')$ transition has been depicted by normalizing the absorption intensities to that of the stronger peak at 981.4 nm. The different evolution of the two peaks with Yb^{3+} concentration indicates that these two lines correspond to two spectroscopically non-equivalent active Yb^{3+} centres in YAB crystal, hereafter labelled as Yb1 and Yb2, whose zero-phonon $^2F_{7/2}(0) \rightarrow {}^2F_{5/2}(0')$ transitions lie at 981.4 and 980.2 nm, respectively.

The absorption area of each one of these two $(0) \rightarrow (0')$ transitions relative to the total area of both zero-phonon lines has been plotted in figure 4 as a function of Yb^{3+} concentration in the crystal. As can be observed, when increasing the ytterbium concentration, the relative area of the zero-phonon line associated with the minor Yb2 centre increases, while that associated with the major Yb1 centre decreases. This behaviour indicates that the incorporation of Yb^{3+} ions in YAB crystals is accompanied by changes in the occupancy distribution into Yb1 and Yb2 centres. For the lowest concentration used in this work, the line associated with the Yb2 centre is hardly detected (see figure 2), and it is expected that for even lower concentrations only Yb1 centres are present in this crystal. Additionally, the different techniques used during the crystal growth process could also affect the relative Yb^{3+} distribution of the two centres in these crystals. As an example, in the spectrum reported in [21], corresponding to a sample of a different origin, the line associated with the Yb2 centre is the dominant one, opposite to our case. Moreover, very recent electron paramagnetic resonance (EPR) results have shown

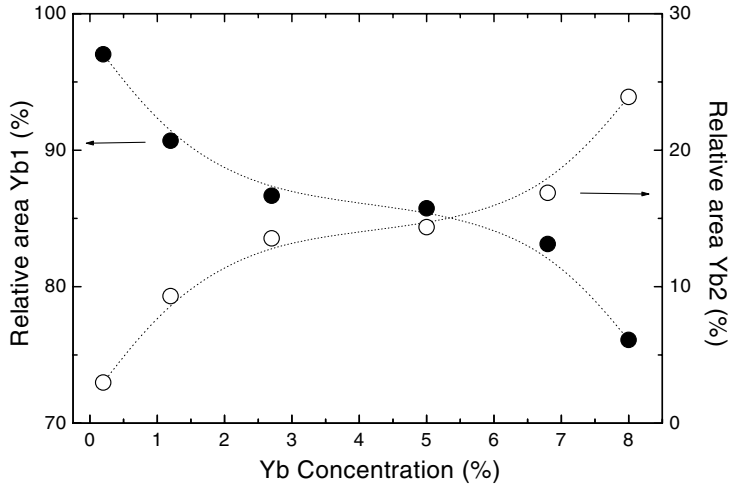

Figure 4. Absorption area of the $^2F_{7/2}(0) \rightarrow {}^2F_{5/2}(0')$ transitions for Yb1 (●) and Yb2 (○) centres relative to the total area of both transitions. The dotted curves are guidelines.

only one Yb^{3+} centre (yttrium site) for nominal concentrations of 0.01 Yb^{3+} atom per YAB molecule in samples grown by the high-temperature top-seeded solution method [25]. Then, the interest of the identification of different lattice centres could constitute a previous step to control, during the growth process, the distribution of active centres in a host laser material of high interest as is the YAB crystal.

It is important to mention here that, despite the fact that a two centre structure must be also present for the remaining zero-phonon $^2F_{7/2}(0) \rightarrow {}^2F_{5/2}(1', 2')$ transitions, the complexity of the spectra in those regions, due to the presence of phonon sidebands, makes impossible their resolution. Additionally, and in agreement with that, the assignment of the characters of the Stark sublevels of the $^2F_{5/2}$ excited state of the previous section has been carried out on the assumption that the main lines observed are those associated with the major Yb1 site. The energy positions and characters of the Stark sublevels for the minor Yb2 centres could not be obtained from the absorption spectra.

As far as the effect of Nd^{3+} co-doping, from the trend obtained in figures 2–4, it is clear that for the adopted Nd^{3+} concentrations levels, the optical absorption of Yb^{3+} ion is not affected. This is important from the viewpoint of using Nd:Yb co-doped crystals in which efficient energy transfer has been reported previously by the authors [26].

Finally, some additional information on the Yb^{3+} incorporation can be obtained from the evolution of the central $^2F_{5/2}(0) \rightarrow {}^2F_{7/2}(1')$ absorption band in the σ spectra when the Yb^{3+} concentration is increased, as can be observed in figure 2. The intensity of the narrow line at 975.4 nm increases up to concentrations around 5 at.% from which a decrease is produced. This reduction in intensity is accompanied by an increase of the width of this line. This behaviour could be related to an increasing inhomogeneous broadening as a consequence of the disorder induced by a higher Yb^{3+} content in the crystal.

3.2. Fluorescence spectra

Figure 5 shows the unpolarized LT (10 K) emission spectrum upon non-selective excitation in the $^2F_{7/2}(0) \rightarrow {}^2F_{5/2}(2')$ transition (935 nm). It consists of four main regions located at around 980, 990, 999 and 1040 nm, which can be associated with the transitions from the

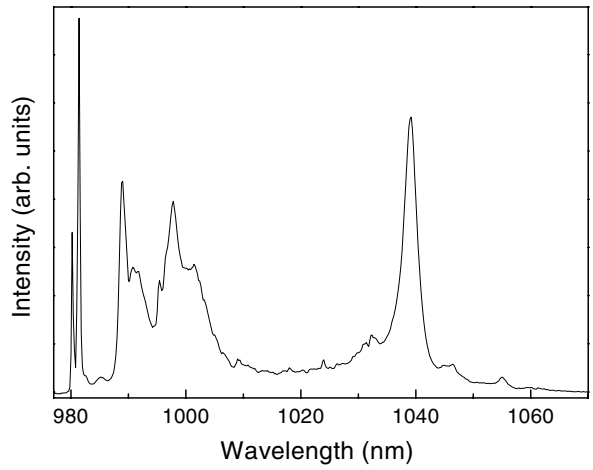

Figure 5. LT (10 K) emission spectra of Yb:YAB crystal (sample 3) under excitation at $\lambda = 935$ nm.

lowest Stark energy level of the excited $^2F_{5/2}(0')$ state to each one of the four Stark sublevels of the $^2F_{7/2}$ ground state.

The spectrum shows two well resolved narrow peaks at 981.4 and 980.2 nm, located at the same energy positions as those detected in the LT absorption spectra at the $^2F_{7/2}(0) \rightarrow {}^2F_{5/2}(0')$ transition region. In fact, the emissions at 981.4 and 980.2 nm correspond to each of the zero-phonon $^2F_{5/2}(0') \rightarrow {}^2F_{7/2}(0)$ transitions of the two non-equivalent spectroscopically Yb1 and Yb2 centres, respectively.

3.2.1. Site selective emission and excitation spectroscopy. In order to obtain additional information, LT excitation spectra have been recorded in the region associated with the $^2F_{7/2}(0) \rightarrow {}^2F_{5/2}(1', 2')$ transitions. Figure 6 shows the results obtained for sample 3 when monitoring at 981.4 and 980.2 nm, that is, those emissions related to the $^2F_{5/2}(0') \rightarrow {}^2F_{7/2}(0)$ transitions of the Yb1 and Yb2 centres, respectively. As can be observed, the spectra are substantially different, which implies different energy level schemes for each Yb^{3+} centre. The spectra have been normalized to the maximum intensity for the sake of clarity; the intensity of the Yb1 centre is about ten times higher than for the Yb2 centre.

The excitation spectra corresponding to the Yb1 centre is in good agreement with the absorption spectra shown in figures 1 and 2. This confirms the fact that the contribution of the Yb1 centre dominates the absorption spectra (except for that well resolved line at 980.2 nm associated with the minor Yb2) and corroborates that the character of the Stark sublevels previously obtained from the absorption spectra is, in fact, associated with the Yb1 major centre.

The excitation spectra monitoring the emission from the Yb2 centre ($\lambda_{em} = 980.2$ nm) shows mainly two bands located at 964.5 and 932 nm. These bands can be related to the $^2F_{7/2}(0) \rightarrow {}^2F_{5/2}(1', 2')$ transitions from Yb2 centre, allowing the determination of the energy positions of the Stark sublevels of the $^2F_{5/2}$ excited state for this Yb2 centre.

Site selective emission spectroscopy at 10 K can be used to determine the energy sublevels of the ground $^2F_{7/2}$ state. Thermal population of the excited state Stark sublevels of the $^2F_{5/2}$ is not expected at this temperature, which notably simplifies the spectra and allows us to obtain better information on the optical transitions associated with each Yb^{3+} centre.

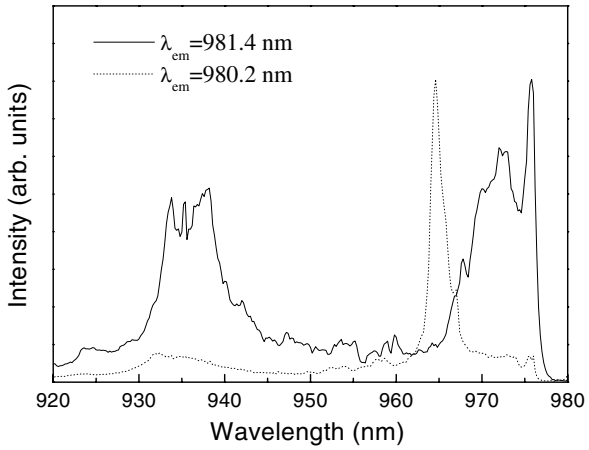

Figure 6. LT (10 K) site selective excitation spectra of Yb^{3+} ions in YAB (sample 3).

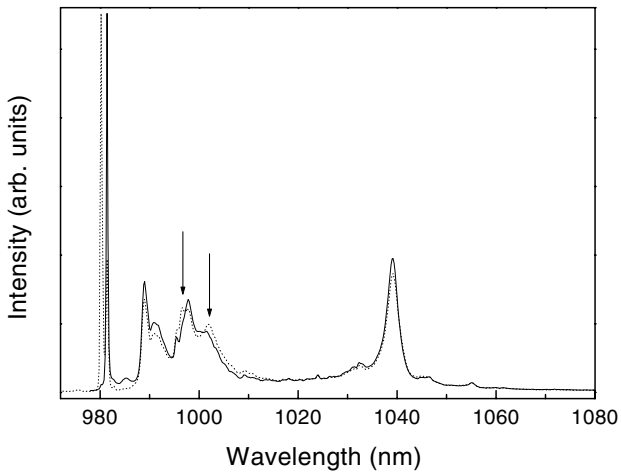

Figure 7. LT (10 K) site selective emission spectra of Yb^{3+} ions in YAB crystal (sample 3).

Figure 7 shows the LT emission spectra associated with the $^2F_{5/2} \rightarrow {}^2F_{7/2}$ transition of Yb^{3+} ions under excitation at the Yb1 centre (975 nm) and Yb2 (964.5 nm), according to the excitation spectra. The spectra have been normalized to the intensity of the zero-phonon $(0') \rightarrow (0)$ line.

As expected, the main difference between those emission spectra is the different position of $^2F_{5/2}(0') \rightarrow {}^2F_{7/2}(0)$ transitions at 981.4 and 980.2 nm from the two Yb1 and Yb2 centres, respectively. The remaining part of the spectra related to the $^2F_{5/2}(0') \rightarrow {}^2F_{7/2}(1, 2, 3)$ transitions show in principle a similar shape. Additionally, this region of the spectra is very similar to that showed in the emission spectra of figure 5 where both centres were simultaneously excited. From this fact, we can conclude again that, except for the $0' \rightarrow 0$ lines, the main contribution to the emission spectra is provided from the major Yb1 centre. The resolution of the particular $^2F_{5/2}(0') \rightarrow {}^2F_{7/2}(1, 2, 3)$ transitions associated with the Yb2 centre appears as a difficult task, furthermore, if we consider that electron–phonon coupling leads to important vibronic broadening of the optical transitions from Yb1, masking the lines related to Yb2 centre. In fact, the assignment of the Yb^{3+} crystal field levels is usually

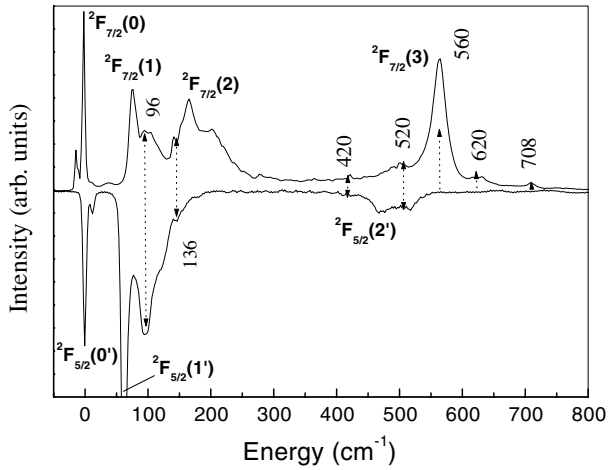

Figure 8. Comparison between the LT (10 K) emission spectrum (positive part) and the σ polarized absorption spectrum (negative part) of Yb:YAB for sample 3. The spectra have been shifted in energy to the zero-phonon $^2F_{7/2}(0) \leftrightarrow {}^2F_{5/2}(0')$ transitions at 10 188 cm^{-1} ($\lambda = 981.4$ nm). The energy of the Raman modes have been marked in the figure.

affected by a certain ambiguity, particularly if different Yb^{3+} centres are present in the host crystal [27–29].

However, when exciting the Yb2 centre some light changes in the $^2F_{5/2}(0') \rightarrow {}^2F_{7/2}$ (1, 2, 3) transition regions, such as an enhancement of the emitted intensity at 996.6 and 1002 nm (marked with arrows in the figure), are obtained. This could indicate that two Stark energy levels corresponding to Yb2 centre could be located at these energies.

Finally, although the spectra shown in this section correspond to a 2.5% Yb^{3+} doped sample it is important to mention that no new lines or significant changes in the spectra are observed when increasing the Yb^{3+} concentration up to 8 at.%. Even though the amount of Yb2 centres is higher in the most concentrated sample, (see figure 4), the Yb1 centre is still the dominant one, and its broad bands, the consequence of the strong electron–phonon interaction, govern the emission spectrum. Thus, the complete characterization of Yb2 centre cannot be obtained by spectroscopic measurements, and additional techniques such as EPR and/or Rutherford back scattering (RBS) are needed.

3.3. Vibrational structure

When two Yb^{3+} centres are present, the vibrational modes should normally couple to the zero-line transitions of each centre. However, in our case the different intensities of the two zero-phonon $^2F_{7/2}(0) \rightarrow {}^2F_{5/2}(0')$ absorption lines for each centre (see figure 2) suggest, as previously pointed out, that mainly the vibronic sidebands from the dominant Yb1 centre contribute significantly to the spectra. Therefore, by choosing the energy of the zero-phonon $^2F_{5/2}(0') \leftrightarrow {}^2F_{7/2}(0)$ transitions of the Yb1 centre as reference (10 188 cm^{-1}, 981.4 nm), we have represented in figure 8 the LT absorption and the emission spectra plotted as a function of the energy in wavenumber. The abscissa corresponds to the absolute energy difference between the absorbed/emitted photon and the transition involving the lowest crystal field components of the ground and excited states, $^2F_{5/2}(0') \leftrightarrow {}^2F_{7/2}(0)$.

By comparing the absorption and emission spectra, it may be possible to identify some of the vibronic sidebands relative to Yb1 centres, since they should appear as symmetrical twins

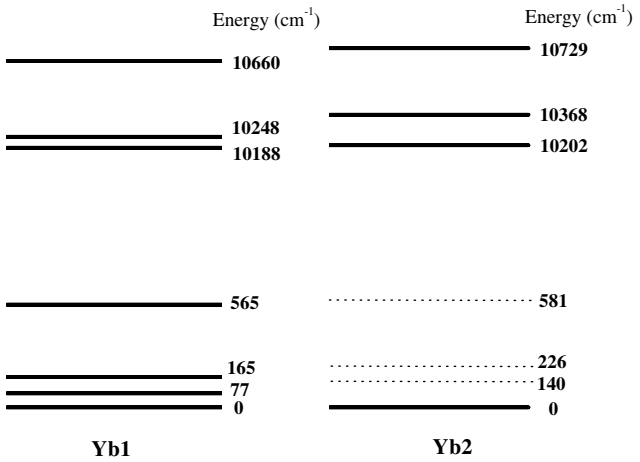

Figure 9. Crystal field splitting schemes associated with Yb1 and Yb2 centres in YAB crystal. The ground state level of Yb2 centre is dotted because it should be considered as preliminary.

relative to the zero-phonon $^2F_{5/2}(0') \leftrightarrow {}^2F_{7/2}(0)$ transitions of the absorption and emission spectra [30]. In fact, as observed in figure 8, a symmetrical arrangement of the spectral structure relative to the zero-phonon $^2F_{5/2}(0') \leftrightarrow {}^2F_{7/2}(0)$ electronic transitions is observed. Particularly, in the 80–150 cm^{-1} range the spectral features appearing at 96 and 136 cm^{-1} (marked with arrows in the figure) can be clearly associated with vibronic sidebands connected to the zero-phonon line of the $^2F_{7/2}(0) \leftrightarrow {}^2F_{5/2}(0')$ transitions. These energy positions can be well related to the Raman active normal modes of YAB. As a matter of fact, previous studies on the vibrational spectra in YAB crystals have shown the presence of optical phonon modes at around 90 and 130 cm^{-1}, which have been associated with external vibration of the BO_3 and AlO_6 groups against the Yb/Y ions. Internal vibrations of those groups have also been identified by Raman spectroscopy at 420, 520, 620 and 700 cm^{-1} [31]. These lattice vibrations are also clearly observed in figure 8 modulating our optical spectra. Moreover, a lattice vibration at 562 cm^{-1} has been detected in the Raman spectra of YAB crystals. The energy match between the this mode and the $^2F_{7/2}(3)$ electronic level could enhance the electronic transition terminating at this crystal field level.

It should be noted that an optical phonon of very low energy, around 60 cm^{-1}, could also be involved. This phonon could be responsible of the structure observed in the π absorption spectrum at 975.2 and 969 nm for which the selective excitation provide two emission spectra completely similar to that corresponding to Yb1 centre. Further experimental work in order to obtain more information on this topic it is now the subject of study.

Once the most important vibronic components have been identified, and taking into account the results of the optical absorption and site selective spectroscopy, the crystal field energy level diagram corresponding to the different Yb^{3+} centres in YAB crystals has been obtained and it is shown in figure 9. The different nature of the two centres present in the crystal is clearly confirmed from the difference in the energy level splitting of the $^2F_{5/2}$ excited state for both Yb1 and Yb2 centres. On the other hand, the splitting of the $^2F_{7/2}$ ground state proposed for the Yb2 centre should be considered as preliminary due to the complexity of the emission spectra. (We have plotted it as dotted lines in figure 9.)

The major Yb1 centre detected in our work can be associated with Yb^{3+} ions located at the regular Y^{3+} lattice positions with D_3 symmetry sites, in agreement with previous studies on different trivalent rare earth doped YAB crystal.

The determination of the origin of the Yb2 centre appears as a complex subject and several explanations could account for the presence of an additional Yb^{3+} centre. Previous results on EuAB crystals ($EuAl_3(BO_3)_4$), demonstrating the presence of different types of Eu^{3+} centres (three), have related the non-regular lattice centres to Al^{3+} or interstitial sites [32]. On the other hand, Er^{3+} doped YAB crystals also show the presence of additional lattice sites that may originate from either Er–Er or Er–crystal defect interactions at high dopant concentrations [21]. This could be the situation for our Yb2 centre, which could be related to slightly distorted Y^{3+} sites due to the aforementioned effects. Also, the existence of growth defects related to the crystal structure of YAB could play a role in the presence of the Yb2 centre. The crystal structure is built of layers of BO_3 group with Y^{3+} and Al^{3+} ions located in the interstices of these layers [33, 34]. Due to the large spacing between the layers, some unavoidable impurities from the flux, such as K^+, could enter these interstices and be responsible for a possible distortion of the regular Y^{3+} sites.

In any case, once the presence of the non-regular site for Yb^{3+} in the YAB crystal has been demonstrated, its origin deserves additional attention. Its definitive nature cannot be determined from optical measurements and additional experiments, such as EPR in the concentration range in which the Yb2 centre is observed, should be used to confirm their local symmetry.

4. Conclusion

We have carried out a detailed spectroscopic study of Yb^{3+} ions in YAB. LT polarized absorption spectra have been used to determine the character of the Stark sublevels corresponding to the $^2F_{5/2}$ state. From the detailed analysis of LT absorption spectra, two different Yb^{3+} centres have been determined and their contribution to the total absorption spectra has been obtained in a wide range of concentrations (0.2–9 at.%), showing that when the total ytterbium concentration is increased, the presence of Yb2 centres is increased with respect to the total ytterbium centres. Site selective excitation and emission experiments combined with the analysis of electron–phonon coupling led us to obtain the energy level diagram corresponding to each centre.

Acknowledgments

This work was carried out in the frame of a Spain–Italy Integrated Action cooperative project. This work has been supported by the Comunidad Autónoma de Madrid (CAM) under Project No. 07N/0020/2002 and by the Comisión Interministerial de Ciencia y Tecnología (CICYT) under project No. MAT2001-0167. The authors gratefully thank Erica Viviani (DST, University of Verona) for expert technical assistance. D Jaque thanks the Ministerio de Ciencia y Tecnología of Spain for a Ramon y Cajal contract.

References

[1] Ellens A, Andre H, Ter Heerdt M L H, Wegh R T, Meijerink A and Blasse G 1996 *J. Lumin.* **66/67** 240
[2] Lupei A, Lupei V, Enaki V N, Presura C and Petraru A 1999 *Spectrochim. Acta* A **58** 773
[3] Druon F, Chenais S, Raybaut P, Balembois F, Georges P, Gaume R, Aka G, Viana B, Vivien D, Chambaret J P, Mohr S and Kopf D 2002 *Opt. Mater.* **19** 73
[4] Chenais S, Druon F, Balembois F, Georges P, Gaume R, Haumesser P H, Viana B, Aka G P and Vivien D 2002 *J. Opt. Soc. Am.* B **19** 1083
[5] Montoya E, Sanz-García J A, Capmany J, Bausá L E, Diening A, Kellner T and Huber G 2000 *J. Appl. Phys.* **87** 4056
[6] Filimonov A A, Leonyuk N I, Meissner L B, Timchenko T I and Rez I S 1974 *Krist. Tech.* **9** 63

[7] Chen Y F, Wang S C, Kao C F and Huang T M 1996 *IEEE Photonics Technol. Lett.* **8** 1313
[8] Omatsu T, Kato Y, Shimosegawa M, Hasegawa A and Ogura I 1995 *Opt. Commun.* **118** 302
[9] Jaque D, Capmany J and Garcia-Solé J 1999 *Appl. Phys. Lett.* **75** 325
[10] Jaque D, Capmany J and Garcia Solé J 1999 *Opt. Eng.* **38** 1794
[11] Wang P, Dawes J M, Dekker P and Piper J A 2000 *Opt. Commun.* **174** 467
[12] Wang P, Dekker P, Dawes J M, Piper J A, Liu Y and Wang J 2000 *Opt. Lett.* **25** 731
[13] Dekker P, Dawes J M, Piper J A, Liu Y and Wang J 2001 *Opt. Commun.* **195** 431
[14] Burns P A, Dawes J M, Dekker P, Piper J A, Li J and Wang J 2002 *Opt. Commun.* **207** 315
[15] Dekker P, Burns P A, Dawes J M, Piper J A, Li J, Hu X and Wang J 2003 *J. Opt. Soc. Am.* B **20** 4
[16] Wang P, Dawes J M, Dekker P, Knowles D S, Piper J A and Lu B 1999 *J. Opt. Soc. Am.* B **16** 63
[17] Bartl M H, Gatterer K, Cavalli E, Speghini A and Bettinelli M 2001 *Spectrochim. Acta* A **57** 1981
[18] Belokoneva E L, Azizov A V, Leonyuk N I, Simonov M A and Belov N V 1981 *Zh. Strukt. Khim.* **22** 196
[19] Földvári I, Beregi E, Munoz A, Sosa R and Horbath V 2002 *Opt. Mater.* **19** 241
[20] Henderson B and Imbusch G F 1989 *Optical Spectroscopy of Inorganic Solids* (Oxford: Clarendon)
[21] Földvári I, Beregi E, Baraldi A, Capelleti R, Ryba-Romanowski W, Dominiak-Dzik G, Munoz A and Sosa R 2003 *J. Lumin.* **102/103** 395
[22] Hehlen M P, Kuditcher A, Rand S and Tischler M 1997 *J. Chem. Phys.* **107** 13
[23] Lupei A, Lupei V, Presura C, Enaki V N and Petraru A 1999 *J. Phys.: Condens. Matter* **11** 3769
[24] Montoya E, Agulló-Rueda F, Manotas S, García Solé J and Bausá L E 2001 *J. Lumin.* **94/95** 701
[25] Watterich A, Aleshkevych P, Borowiec M T, Zayarnuk T, Szymezak H, Beregi E and Kovács L 2003 *J. Phys.: Condens. Matter* **15** 3323
[26] Jaque D, Ramirez M O, Bausá L E, García Solé J, Cavalli E, Speghini A and Bettinelli M 2003 *Phys. Rev.* B **68** 035118
[27] Bogomolova G A, Vylegzhanin D N and Kaminskii A A 1976 *Sov. Phys.—JETP* **42** 440
[28] Acevedo R, Tanner P A, Meruane T and Poblete V 1996 *Phys. Rev.* B **54** 3976
[29] Mougel F, Dardenne K, Aka G, Kahn-Harari A and Vivien D 1999 *J. Opt. Soc. Am.* B **16** 164
[30] Buchanan R A, Wickersheim K A, Pearson J J and Hermann G F 1967 *Phys. Rev.* **159** 245
[31] Xia H R, Li L X, Wang J Y, Yu W T and Yang P 1999 *J. Raman Spectrosc.* **30** 557
[32] Kellendonk F and Blasse G 1981 *J. Chem. Phys.* **75** 561
[33] Mills A 1962 *Inorg. Chem.* **1** 960
[34] Wang J, Hu X, Liu H, Li J, Jiang S, Zhao S, Teng B, Tian Y and Jiang J 2001 *J. Cryst. Growth* **229** 256